

Supplementary Material

Unusual sulfide-rich magmatic apatite crystals from >2.7 Ga Abitibi Greenstone Belt, Canada

**Xuyang Meng^{1,2,3*}, David R. Mole⁴, Adam C. Simon², Jingwen Mao¹, Daniel J. Kontak³,
Pedro J. Jugo³, Jackie M. Kleinsasser²**

¹ School of Earth Sciences and Resources, China University of Geosciences, Beijing 100083, China

² Department of Earth and Environmental Sciences, University of Michigan, Ann Arbor, Michigan 48109, USA

³ Mineral Exploration Research Centre, Harquail School of Earth Sciences, Laurentian University, Sudbury, Ontario P3E 2C6, Canada

⁴ Geoscience Australia, Mineral Systems Branch, Canberra, ACT, Australia

*Corresponding author. Email: xmengl@cugb.edu.cn

This PDF file includes:

1. Samples and analytical methods
2. Source of the compiled data
3. P-T correction of magmatic fO_2 estimated from S-in-apatite oxybarometer
4. Method in estimating melt S concentration
5. References

Other Supplementary Materials for this manuscript include the following:

Supplementary Figure 1 (Figure S1)
Supplementary Figure 2 (Figure S2)
Supplementary Table 1 (Table S1)
Supplementary Table 2 (Table S2)
Supplementary Table 3 (Table S3)
Supplementary Table 4 (Table S4)
Supplementary Table 5 (Table S5)

1. Samples and analytical methods

Apatite inclusions were identified in zircon grains concentrated in previous studies (see Mole et al., 2021) extracted from 28 samples of >2695 Ma volcanic rocks across the Abitibi greenstone belt in the Neoproterozoic Superior Province (Fig. 1a) using a Tescan Vega 3 scanning electron microscope (SEM) equipped with a Bruker energy-dispersive spectrometer (EDS) at Laurentian University. We restrict to analyze the apatite inclusions that are remote from fractures in the zircon grains for minimizing any potential effects from metamorphism and hydrothermal alteration.

1.1. Whole-rock geochemistry

Twelve representative samples of pre-tectonic volcanic rocks were crushed and ground at Australian Laboratory Services (ALS), Sudbury, Canada for whole-rock geochemical analyses. The powdered samples were analyzed using X-ray fluorescence (XRF) and inductively coupled plasma-mass spectrometry (ICP-MS) with pre-fusion by lithium metaborate (following CCP-PKG03 analytical package) at ALS, Vancouver, Canada. To monitor data accuracy and precision, four samples of two secondary reference materials (LK-NIP-1, Nipissing diabase; and IAG ORPT-1 Rhyolite) were included as unknown samples in the submitted samples for analysis and the results are consistent with published values (see Supplementary Table 2).

1.2. Electron probe microanalysis (EPMA)

The major and trace elements of the apatite inclusions were acquired with a Cameca SX100 electron microprobe analyzer operated using the wavelength-dispersive spectrometry (WDS) method at the Ontario Geoscience Laboratories (GeoLabs, Sudbury, Ontario). Fourteen elements (P, Si, Al, Mg, Ca, Mn, Fe, Sr, Na, K, S, F, Cl, Zr) were measured using the following conditions: 15-kV accelerating voltage, 10-nA beam current, and 2- or 5- μ m raster beam sizes. X-ray lines, analyzing crystals, counting times (for both peak and background measurements), were as follows: P K α , LPET5, 15 s; Si K α , LTAP2, 20 s; Al K α , LTAP2, 20 s; Mg K α , LTAP2, 20 s; Ca K α , LPET5, 15s; Mn K α , LiF4, 40s; Fe K α , LiF4, 40s; Sr L α , LPET5, 30s; Na K α , LTAP2, 20s; K K α , PET3, 20s; S K α , LPET3, 60s; F K α , PCO, 5s; Cl K α , LPET5, 20 s; Zr L α , LPET5, 5 s. The detection limits for these elements were calculated to be as follows: P₂O₅, 930 ppm; SiO₂, 210 ppm; Al₂O₃, 190 ppm; MgO, 200 ppm; CaO, 480 ppm; MnO, 930 ppm; FeO, 770 ppm; SrO, 1230 ppm; Na₂O, 250 ppm; K₂O, 210 ppm; SO₃, 310 ppm; F, 1850 ppm; and Cl, 250 ppm. Zirconium concentrations were measured to monitor the contamination of the apatite by the host zircon; analyses with >1 wt. % ZrO₂ were excluded. As previously reported in Meng et al. (2021a), the S and Cl contents have been tested to be reliable, but F content in apatite (~20 seconds) may be compromised by decomposition using a 2 μ m beam. During our analyses, we used a 5 second acquisition for F to minimize the decomposition but the precision for the F may be affected. Damage of apatite using a beam size of 5 μ m can be minimized, particularly for

apatite grains with the *c*-axis perpendicular to the electron beam. The results are reported in Supplementary Table 3.

1.3. Micro X-ray absorption near edge structure (μ -XANES) at the S K-edge

Micro X-ray absorption near-edge structure spectroscopy at the sulfur K-edge (S μ -XANES) was conducted to measure the sulfur oxidation states of apatite inclusions at the Advanced Photon Source (APS) of the Argonne National Laboratory in Chicago, IL, USA. The analyses were performed at the GSECARS X-ray microprobe beamline on sector 13-ID-E, which has an energy range of 2.3–28 keV and uses double crystal (silicon 111) monochromators to generate monochromatic radiation focused with a Kirkpatrick-Baez mirror system. The energy at the beamline was calibrated to the \sim 2482 eV white line of sulfate using clear double-sided sticky tape at APS (2481.8 eV). Details of the method used in analyzing zircon-hosted apatite inclusions are provided in Meng et al. (2021a) and Meng et al. (2022).

The μ -XANES analyses were conducted on representative apatite crystals unaffected by prior electron microprobe beam analysis. X-ray fluorescence (XRF) maps were collected at the beamline immediately preceding spectra collection to locate the apatite inclusions. The sulfur fluorescence spectra were collected using four-element silicon drift diode detector arrays positioned at an angle of 90° to the incident beam and corrected for detector and electronics dead time. Two scans were collected at each point to improve counting statistics and to monitor for beam damage caused by irradiation of the focused X-ray beam and contribution from other phases (e.g., the host zircon, epoxy). The effective beam size is $2 \times 2 \mu\text{m}^2$. The S μ -XANES spectra were collected by scanning the incident beam energy from 2440 to 2550 eV, and the scan can be divided into three energy regions: i) a pre-edge background region from 2440–2460 eV; ii) the edge region from 2460–2500 eV, and iii) a post-edge region from 2500–2550 eV. Step sizes of 1, 0.3 eV, and 2 eV were used in the pre-edge, edge, and post-edge regions, respectively, with counting duration of 3 s for all regions. The S K-edge XANES spectra database from the European Synchrotron Radiation Facility was used to identify the S^{6+} (\sim 2482 eV; anhydrite), S^{4+} (\sim 2478 eV; sodium sulfite), and S^{2-} (\sim 2470 eV; pyrrhotite) peak energy position for the unknowns.

Beam damage was not observed in any apatite spectra collected in this study, consistent with previous observations that apatite does not easily incur beam damage at the energies for S μ -XANES analyses even after 1 hour of beam exposure (Konecke et al., 2017). One spectrum was only obtained for one apatite grain from sample C83-16, and the data is not reported in the main text. Contributions of zircon and sulfur-bearing epoxy to the S μ -XANES spectra were monitored following the criteria described in Konecke et al. (2019) and Meng et al. (2021a), and any spectra with contamination from other phases were discarded. The S μ -XANES spectra normalized against the incident flux (I_0), the pre- and post-edge set to 0 and 1, respectively. The spectra for the same apatite grains were merged using the XAS software analysis package Athena

or Ifeffit (Ravel and Newville, 2005). Peak positions and areas were then fitted and calculated using the Fityk software version 1.3.1 (Wojdyr, 2010). An exponentially modified Gaussian (EMG) cumulative distribution was fit the subtract the background, whereas the Gaussian area curves fit to each peak, from which the integrated $S^{6+}/\Sigma S$ peak area ratios were calculated and used for estimating fO_2 values at the time of apatite crystallization.

2. Source of the compiled data

The whole-rock geochemistry data were compiled by Mole et al. (2021) from online public datasets, including (i) GEOROC online database (Sarbas, 2008); (ii) Ontario Geological Survey miscellaneous-release data MRD285 (Beakhouse, 2011), MRD143 (Ayer et al., 2004), MRD282 (Ayer et al., 2011); and (iii) Ministère des Ressources Naturelles du Québec (MERN) online dataset (SIGEOM). The compiled datasets have been classified (Mole et al., 2021), and we only used the whole-rock geochemistry data for the TTG and volcanic rocks with accurate coordinates. The recently published lithogeochemistry data (Meng et al., 2021b) were also included. We filtered the data using criteria as follows: (1) $LOI \leq 2$ wt. %, (2) $55 \text{ wt. \%} \leq SiO_2 \leq 75 \text{ wt. \%}$, in which the SiO_2 contents were calculated on the anhydrous basis. The data for the sodic TTG and volcanic rocks were filtered to remove those with $K_2O/Na_2O \geq 0.6$. Using the filtering criteria, we obtained a total of 2316 data points for the sodic TTG and volcanic rocks.

The U-Pb-Hf-O isotopes and trace element abundances for these zircon samples have previously been reported (Mole et al., 2021) and are reused. The zircon trace element data were filtered using criteria as follows: (1) La content < 1 ppm; (2) LREE Index ($LREE-I = (Dy/Nd) + (Dy/Sm) > 10$); (3) Ti content $>$ detection limit and < 50 ppm; (4) age discordance < 10 % (Lu, 2016; Bell et al., 2016; Meng et al., 2021b).

3. P-T correction of magmatic fO_2 estimated from S-in-apatite oxybarometer

In silicate melts, changes in temperature and pressure can shift the sulfide-sulfate transition in fO_2 space for silicate glasses. A decrease in temperature of 100°C and pressure of 300 MPa have experimentally been suggested to result in a deviation of $\Delta FMQ + 0.5$ and -0.2 , respectively (Matjuschkin et al., 2016; Nash et al., 2019). We consider the effect of temperature and pressure on silicate melts proportional to the effect of sulfur incorporation into apatite (Konecke et al., 2019; Meng et al., 2021; Meng et al., 2022). Because the S-in-apatite oxybarometer is calibrated at a temperature of 1000°C and 300 MPa, we corrected the magmatic fO_2 estimated from the S-in-apatite oxybarometer by evaluating the pressure and temperature at which the zircon-hosted apatite inclusions crystallized. A simple linear equation is described as:

$$fO_2(\Delta FMQ)_{Corrected} = fO_2(\Delta FMQ)_{calculated} + 0.5 * (1000 - T_{apatite})/100 - 0.2 * (300 - P_{apatite})/300$$

in which the fO_2 are reported in ΔFMQ values, whereas T_{apatite} ($^{\circ}\text{C}$) and P_{apatite} (MPa) are the temperature and pressure at the time of apatite crystallization.

The zircon-hosted apatite crystals from the volcanic rocks are assumed to crystallize at pressure over a range from that for the TTG batholith (300–700 MPa and locally 100 MPa; Beakhouse et al., 2005, 2011) to near-atmospheric pressure. Apatite inclusions hosted in P-poor phase (e.g., zircon) are generally thought to crystallize in response to local saturation of apatite against the growing mineral surfaces (i.e., zircon) due to the slow diffusivity rate of phosphorus in silicate melts (Green and Watson, 1982; Bell et al., 2022), the maximum temperature at the time of the zircon crystallization is therefore used to approximate the crystallization temperature of the apatite grains. In addition, apatite saturation thermometry is employed to estimate the temperature at which the apatite began to crystallize (Piccoli and Candela, 1994), we calculated the *model* apatite saturation temperature using whole-rock SiO_2 and P_2O_5 contents on an anhydrous basis (Piccoli and Candela, 2002). Because the apatite saturation thermometer is more suitable for metaluminous to slightly peraluminous systems (Piccoli and Candela, 1994), and the SiO_2 and P_2O_5 may be affected by hydrothermal alteration, we filtered the previously compiled geochemical dataset using the following criteria: A/CNK [mole $\text{Al}_2\text{O}_3/(\text{CaO}+\text{Na}_2\text{O}+\text{K}_2\text{O})] \leq 1.1$ and $\text{LOI} < 2.0$ wt. %. The modeled apatite saturation temperatures for the sodic volcanic rocks are calculated at 892 ± 49 $^{\circ}\text{C}$ (SD, $n = 1372$), consistent with the maximum crystallization temperature of the host zircon grains (Fig. S2).

4. Methods in estimating melt S concentration

We used the equation in Meng et al. (2021a) to estimate the S concentration in the silicate melt at the time of apatite crystallization, that is expressed as:

$$S_{\text{melt}} = [S_{\text{ap}}/D_{\text{S}^{\text{ap/m}}}(fO_2)]/[D_{\text{S}^{\text{ap/m}}}(\text{AST})/D_{\text{S}^{\text{ap/m}}}(1000^{\circ}\text{C})]$$

The equation combines (1) the experimental partition coefficient of S between apatite and melt ($D_{\text{S}^{\text{ap/m}}}$) for a mafic melt varying with magmatic fO_2 at a temperature of 1000 $^{\circ}\text{C}$ and pressure of 300 MPa (Koneck et al, 2019); and (2) the temperature-dependent $D_{\text{S}^{\text{ap/m}}}$ for an oxidized rhyolitic melt (Parat and Holtz, 2004). The range of S concentrations in silicate melts for this study is estimated at a temperature of 892 ± 49 $^{\circ}\text{C}$ and a pressure of 0–700 MPa (See details in Table S1).

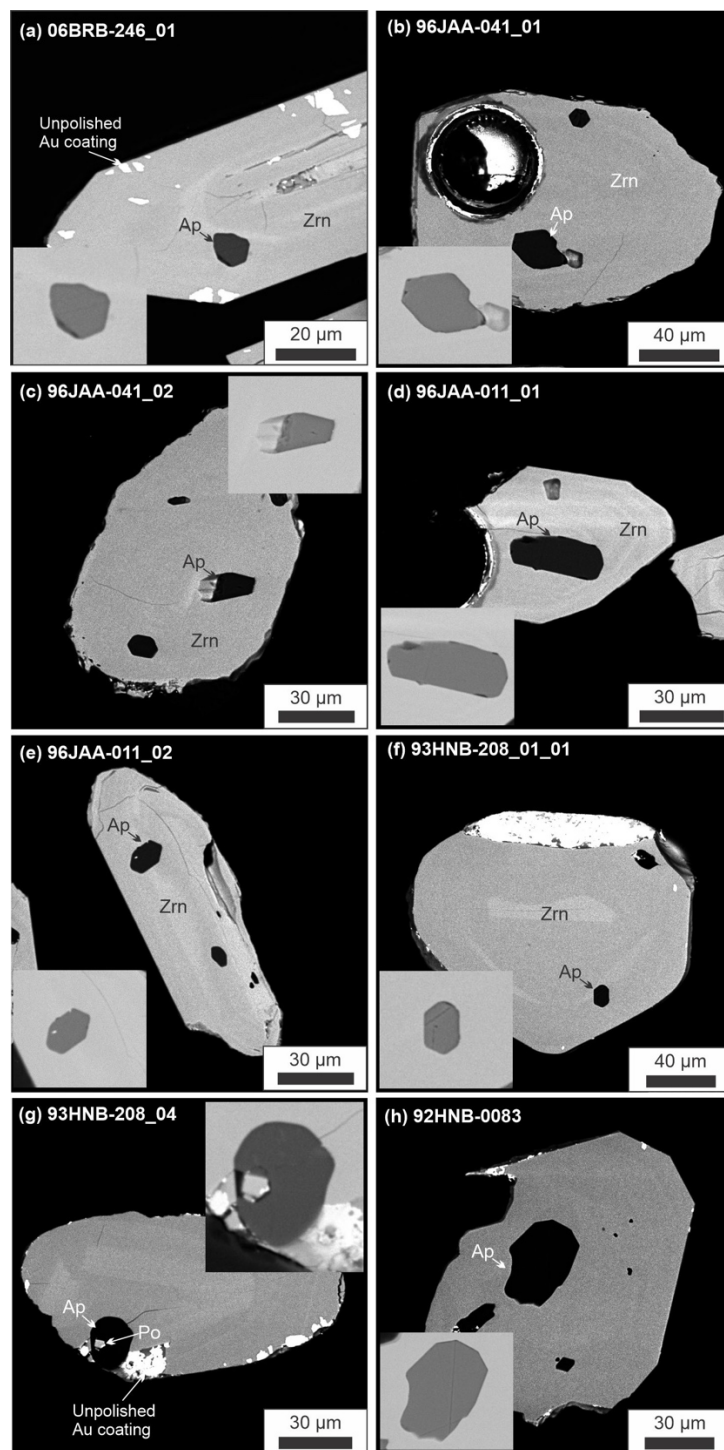


Fig. S1. Backscattered electron images of zircons with apatite inclusions used for μ -XANES analyses that were separated from volcanic rocks from the Abitibi greenstone belt in southern Superior Province. The euhedral pyrrhotite hosted by zircon-hosted apatite inclusion in (g) is interpreted to be of magmatic origin and to form earlier than the apatite host. Abbreviations: Ap = apatite, Po= pyrrhotite, Zrn = zircon. See sample information in Supplementary Table 1.

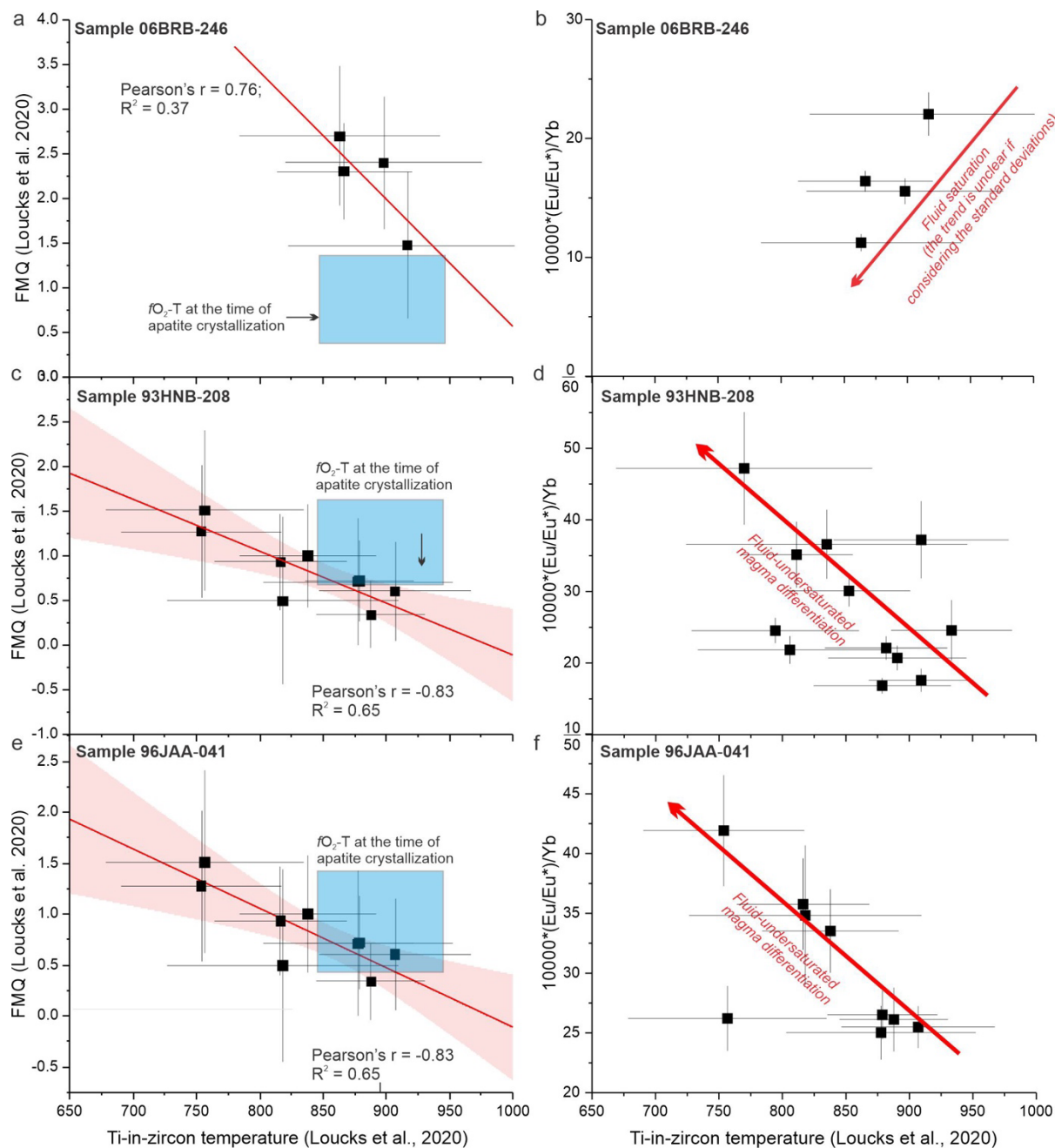


Fig. S2. Magmatic fO_2 in FMQ values and zircon 10000*(Eu/Eu*)/Yb ratio versus temperature estimated using zircon geochemistry for the studied volcanic rocks collected from the Abitibi Greenstone Belt in the southern Superior Province, following the method of Loucks et al. (2020). The FMQ values estimated using a P-T-corrected S-in-apatite oxybarometer and the apatite saturation temperature are plotted for comparison. We note that the estimated FMQ values estimated using zircon U_i-Ti-Ce and S-in-apatite oxybarometers are comparable within uncertainty at a fixed temperature. The results for sample 96JAA-011 are not plotted because only two zircon datapoints are present. See sample information in Supplementary Table 1.

References

- Ayer, J.A., Chartrand, J.E. (2011) in *Miscellaneous Release---Data 282*. O. G. Survey, Ed. (Ontario Geological Survey).
- Ayer, J.A., Trowell, N.F., Josey, S. (2004) in *Miscellaneous Release—Data 143*. O. G. Survey, Ed. (Ontario Geological Survey).
- Bell, E.A., Boehnke, P., and Harrison, T.M. (2016) Recovering the primary geochemistry of Jack Hills zircons through quantitative estimates of chemical alteration: *Geochimica et Cosmochimica Acta*, 191, 187–202.
- Bell, E.A., Kirkpatrick, H.M., and Harrison, T.M. (2022) Crystallization order effects on inclusion assemblages in magmatic accessory minerals and implications for the detrital record: *Chemical Geology*, 613, 121143.
- Beakhouse, G.P., and Davis, D.W. (2005) Evolution and tectonic significance of intermediate to felsic plutonism associated with the Hemlo greenstone belt, Superior Province, Canada: *Precambrian Research*, 137, 61–92.
- Beakhouse, G.P. (2011) The Abitibi Subprovince plutonic record: Tectonic and metallogenic implications: Ontario Geological Survey, Open File, 6268, 1–161.
- Green, T.H., and Watson, E.B. (1982) Crystallization of apatite in natural magmas under high pressure, hydrous conditions, with particular reference to ‘Orogenic’ rock series: *Contributions to Mineralogy and Petrology*, 79, 96–105.
- Konecke, B.A., Fiege, A., Simon, A.C., Parat, F., and Stechern, A. (2017) Co-variability of S^{6+} , S^{4+} , and S^{2-} in apatite as a function of oxidation state: Implications for a new oxybarometer: *American Mineralogist*, 102, 548–557.
- Konecke, B.A., Fiege, A., Simon, A.C., Linsler, S., and Holtz, F. (2019) An experimental calibration of a sulfur-in-apatite oxybarometer for mafic systems: *Geochimica et Cosmochimica Acta*, 265, 242–258.
- Loucks, R.R., Fiorentini, M.L., and Henríquez, G.J. (2020) New magmatic oxybarometer using trace elements in zircon: *Journal of Petrology*, 61, 1–30.
- Lu, Y.J. (2016) Zircon Compositions as a Pathfinder for Porphyry Cu \pm Mo \pm Au Deposits: Society of Economic Geologists Special Publication, 19, 329–347.
- Matjuschkin, V., Blundy, J.D., and Brooker, R.A. (2016) The effect of pressure on sulphur speciation in mid- to deep-crustal arc magmas and implications for the formation of porphyry copper deposits: *Contributions to Mineralogy and Petrology*, 171, 66.
- Meng, X., Kleinsasser, J.M., Richards, J.P., Tapster, S.R., Jugo, P.J., Simon, A.C., Kontak, D.J., Robb, L., Bybee, G.M., Marsh, J.H., and Stern, R.A. (2021a) Oxidized sulfur-rich arc magmas formed porphyry Cu deposits by 1.88 Ga: *Nature Communications*, 12, 2189.
- Meng, X., Richards, J.P., Kontak, D.J., Simon, A.C., Kleinsasser, J.M., Marsh, J.H., Stern, R.A., and Jugo, P.J. (2021b) Variable modes of formation for tonalite–trondhjemite–granodiorite–diorite (TTG)-related porphyry-type Cu \pm Au deposits in the Neoarchean Southern Abitibi Subprovince (Canada): Evidence from petrochronology and oxybarometry: *Journal of Petrology*, 62, 1–29.
- Meng, X., Simon, A.C., Kleinsasser, J.M., Mole, D.R., Kontak, D.J., Jugo, P.J., Mao, J., and Richards, J.P. (2022) Formation of oxidized sulfur-rich magmas in Neoarchean subduction zones: *Nature Geoscience*, 15, 1064–1070.

- Mole, D.R., Thurston, P.C., Marsh, J.H., Stern, R.A., Ayer, J.A., Martin, L.A.J., and Lu, Y.J. (2021) The formation of Neoarchean continental crust in the south-east Superior Craton by two distinct geodynamic processes: *Precambrian Research*, 356, 106104.
- Nash, W.M., Smythe, D.J., and Wood, B.J. (2019) Compositional and temperature effects on sulfur speciation and solubility in silicate melts: *Earth and Planetary Science Letters*, 507, 187–198.
- Parat, F., and Holtz, F. (2004) Sulfur partitioning between apatite and melt and effect of sulfur on apatite solubility at oxidizing conditions: *Contributions to Mineralogy and Petrology*, 147, 201–212.
- Piccoli, P.M., and Candela, P.A. (2002) Apatite in igneous systems, 48, 255–292.
- Piccoli, P., and Candela, P. (1994) Apatite in felsic rocks: a model for the estimation of initial halogen concentrations in the Bishop Tuff (Long Valley) and Tuolumne Intrusive Suite (Sierra Nevada Batholith) magmas: *American Journal of Science*, 294, 92–135.
- Ravel, B., and Newville, M. (2005) ATHENA, ARTEMIS, HEPHAESTUS: data analysis for X-ray absorption spectroscopy using IFEFFIT: *Journal of synchrotron radiation*, 12, 537–541.
- Sarbas, B. The GEOROC database as part of a growing geoinformatics network, *in* *Proceedings Geoinformatics 2008—data to knowledge2008*, USGS, 42–43.
- Wojdyr, M. (2010) Fityk: a general-purpose peak fitting program: *Journal of Applied Crystallography*, 43, 1126–1128.